

Aerofoil Design for Unmanned High-Altitude Aft-Swept Flying Wings

Ahmad Abdulkarim Alsahlan¹, Thurai Rahulan¹

ABSTRACT: In this paper, 12 new aerofoils with varying thicknesses for an aft-swept flying wing unmanned air vehicle have been designed using a MATLAB tool which has been developed in-house. The tool consists of 2 parts in addition to the aerodynamic solver XFoil. The first part generates the aerofoil section geometry using a combination of PARSEC and Bezier-curve parameterisation functions. PARSEC parameterisation has been used to represent the camber line while the Bezier-curve has been used to select the thickness distribution. This combination is quite efficient in using an optimisation search process because of the capability to define a range of design variables that can quickly generate a suitable aerofoil. The second part contains the optimisation code using a genetic algorithm. The primary target here was to design a number of aerofoils with low pitching moment, suitable for an aft-swept flying wing configuration operating at low Reynolds number in the range of about 0.5×10^6 . Three optimisation targets were set to achieve maximum aerodynamic performance characteristics. Each individual target was run separately to design several aerofoils of different thicknesses that meet the target criteria. According to the set of result obtained so far, the initial observation of the aerodynamic performance of the newly designed aerofoils is that the lift/drag ratio in general is higher than that of the existing ones used in many current-generation high-altitude long-endurance aircraft. Another observation is that increasing the maximum thickness of the aerofoil leads to a decrease in the maximum lift/drag ratio. In addition, as expected, this ratio sharply drops after the maximum value of some of these aerofoils.

KEYWORDS: Aerofoil design, Low Re, Swept flying wing.

INTRODUCTION

The flight profiles of high-altitude long-endurance unmanned air vehicles (HALE UAVs), at high altitudes and moderate flight speeds, represent low-Reynolds number operating conditions. The required lift coefficient is high when compared to more conventional lower-altitude aircraft, due to reduced air density. Therefore, the aerofoil section needs to be optimised to generate high lift coefficients with a profile drag as low as possible. The pitching moment (C_m) should also be considered especially for the flying wing configuration with no tail. An additional constraint in the selection of suitable aerofoil sections is the thickness required to hold fuel tanks or batteries and the required structural elements for adequate stiffness. In previous literature, different aerofoils were selected on the basis of a high lift/drag ratio. The swept flying wing configuration is not adopted widely in the literature for high altitude operation. Alsahlani *et al.* (2015) introduced a new aft-swept flying wing solar powered UAV operating at 17 km altitude. An HS520 aerofoil was selected due to its low pitching moment and drag coefficient (C_d). Recently, in July 2015, the Facebook Company revealed its first full-scale solar powered aft-swept flying wing aircraft called Aquila, which is to be used to facilitate internet communications in remote parts of the world (The Guardian 2015). However, there is as yet no detailed information available about this aircraft. Selecting or designing an aerofoil for high altitude aircraft can be affected by several considerations that will be explained briefly:

- Aircraft configuration: stability requirement can affect the aerofoil selection process depending on the layout configuration.
Unswept flying wing aircraft has no stabiliser. It depends on the pressure distribution along the

¹University of Salford – School of Computing, Science and Engineering – Department of Aeronautical Engineering – Salford – United Kingdom.

Author for correspondence: Ahmad Abdulkarim Alsahlani | University of Salford – School of Computing, Science and Engineering – Department of Aeronautical Engineering | Newton Building | Postal code: M5 4WT – Salford – United Kingdom | Email: ahmad.alsahlani@gmail.com

Received: Nov., 10, 2016 | **Accepted:** Jan., 24, 2017

chord-wise direction to achieve 0 pitching moment about its aerodynamic centre. This is achieved by the incorporation of a reflexed trailing edge in order to generate a negative lift force at the trailing edge, but at the cost of reducing the maximum lift coefficient and increasing the drag (Buckstrom 1979; Qin *et al.* 2004). NASA prototypes such as Helios, Centurion, and Pathfinder are examples of this approach.

Aft-swept flying wing aircraft uses an aerofoil with a less reflexed trailing edge to reduce the reduction in the maximum lift coefficient ($C_{l,max}$) since a combination of sweep-back and wash-out is used to supplement the generation of the balancing pitching moment. If the pitching moment is large, a huge amount of sweep or wash-out is needed. Therefore, in general, aerofoils with a small pitching moment is preferable for tailless aircraft (Nickel and Wohlfahrt 1994). This approach has been used in manned flying wing aircraft such as the Northrop Grumman B-2 Spirit and the Horten series of aircraft (Mader and Martins 2012; Li *et al.* 2012). This approach will be the main focus of this paper.

Tailed aircraft can use an aerofoil with high lift/drag ratio and the tail is used for stability but at the cost of additional drag from the empennage. QinetiQ Zephyr, Global Observer, X-HALE, and Boeing Phantom Eye are examples of this approach (Rapinett 2009).

- Low Reynolds number: at low Reynolds number the viscous effects are more dominant which generate high drag and at reduced maximum lift while at higher Reynolds number, the lift/drag ratio improves (Greer *et al.* 2000; Lissaman 1983). At low Reynolds number, the performance of an aerofoil is limited by quicker separation of the boundary layer. Therefore, the flow becomes quite unsteady causing the aerodynamic moment and forces to fluctuate with time (Lei *et al.* 2013). A separation bubble may form within boundary layer causing the transition from laminar to turbulent, according to Fig. 1 (Lei *et al.* 2013; Lissaman 1983). The position of this separation bubble and the intensity depends on the shape of the aerofoil, angle of attack (AoA), and Reynolds number (Greer *et al.* 2000). This has the effect of reducing the gradient of the lift curve whilst increasing drag at the same time (Ma and Liu 2009). The majority of the air resistance comes from the pressure drag over the region of the laminar separation

bubble. After the separation bubble, the flow reattaches to the aerofoil and becomes turbulent flow or may stay separated. If it remains separated, the lift coefficient will sharply drop with a marked increase in the drag coefficient. This usually happens at a Reynolds number of about 70,000 (Hazra and Jameson 2007). Previous studies have shown that there is a critical Reynolds number at about 7×10^4 , where the performance of smooth aerofoils presents a noticeable change in the lift/drag ratio. The smooth aerofoils have a higher lift/drag ratio than rough aerofoils at approximately more than $Re > 10^5$. Thus, below this value, roughness is beneficial because this discontinuity in the surface can help to delay flow separation (McArthur 2007).

- Stiffness of structure and internal volume needed: increasing aerofoil thickness can obviously increase the wing stiffness and reduce wing bending moments sensitivity, which will result in reduced structural weight. Furthermore, it will also provide more space for fuel and payload (Cerra and Katz 2008). In general, thicker wing sections reduce both the maximum lift/drag ratio and the stall angle (Ma and Liu 2009).

Table 1 shows the aerodynamic performance of some aerofoils which are designed for aft-swept and straight flying wing aircraft operating in low Reynolds environment. These results were generated using XFOIL at Re . Among these aerofoils, EPPLER 339 and LA2573A have the highest lift/drag ratio and moderate maximum thickness-to-chord ratio (t/c %). Their stall angles seem to occur near the region where the lift/drag ratio reaches a maximum. LA2573A was used in high altitude prototypes such as Helios and Pathfinder aircraft, which sport straight wings (Kroo 1993). This aerofoil has a positive pitching moment to achieve the stability requirement without the need for either wing sweep or twist.

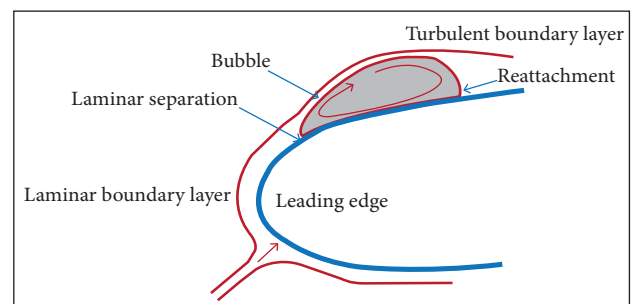


Figure 1. Structure of laminar separation bubble.

Table 1. Number of flying wing aerofoils, at Re , evaluated by XFLR5.

| Aerofoil name | At max C_l/C_d | | | | | C_{lmax} | C_{lmin} | Stall angle | Thickness t/c % |
|---------------|------------------|-------|--------|---------|------------------|------------|------------|-------------|-------------------|
| | C_l/C_d | C_l | C_d | C_m | At AoA \approx | | | | |
| HS 520 | 84.37 | 0.78 | 0.0093 | -0.0022 | 6 | 1.283 | -0.584 | 13 | 9.8 |
| MH 61 | 84.5 | 0.65 | 0.0075 | -0.006 | 5 | 1.03 | -0.62 | 11 | 10.28 |
| EH 2.0/12 | 89.2 | 1.01 | 0.0112 | -0.011 | 8 | 1.2 | -0.8 | 12 | 12 |
| EH 3.0/12 | 93.9 | 1.15 | 0.0123 | -0.005 | 9 | 1.25 | -0.6 | 12 | 12 |
| EPPLER 231 | 95 | 0.845 | 0.009 | -0.052 | 5 | 1.2 | -0.35 | 13 | 12.33 |
| MH 81 | 85.2 | 1.4 | 0.0164 | -0.001 | 11 | 1.65 | -0.5 | 15 | 13 |
| MH 83 | 95 | 1.35 | 0.0142 | -0.064 | 8 | 1.9 | 0.4 | 15 | 13.29 |
| EPPLER 339 | 100 | 1.35 | 0.0135 | -0.045 | 9 | 1.5 | -0.3 | 13 | 13.5 |
| LA2573A | 102 | 1.247 | 0.0122 | 0.0117 | 10 | 1.33 | -0.52 | 12 | 13.7 |
| FAUVEL 14 | 89.3 | 1.15 | 0.0128 | 0.012 | 9 | 1.3 | -0.74 | 11 | 14 |
| EPPLER 342 | 89.3 | 1.39 | 0.0156 | 0.013 | 11 | 1.484 | -0.35 | 13 | 14.3 |
| EPPLER 344 | 94 | 1.41 | 0.015 | -0.032 | 10 | 1.55 | -0.29 | 14 | 14.7 |
| MH91 | 78.9 | 1.07 | 0.0136 | 0.012 | 9 | 1.38 | -0.87 | 16 | 14.98 |
| MH95 | 63.8 | 0.826 | 0.013 | -0.007 | 7 | 1.34 | -0.7 | 17 | 15.86 |

In case of using aft-swept configuration, much attention is paid to the pitching moment of the candidate aerofoil because of the absence of a horizontal stabilizer for stability purposes. Adopting this configuration needs the use of an aerofoil with a smaller pitching moment, but not excessively low in order to obtain a high C_l . Since this configuration has not been adopted in application of high altitude aircraft by the other designers as far as is known, this paper will investigate and design new aerofoils for the 3 aerodynamic targets. The expected operational Reynolds number that is appropriate to similar aircraft is about .

In the literature, 2 main approaches are introduced to design aerofoils, which are based on direct numerical optimisation and inverse design. The common aspect between these 2 approaches is that the aerofoil shape is modified until specific goals are satisfied. For the first approach, the goals are usually the aerodynamic performances characteristic such as the lift, drag, and pitching moment coefficients, whereas the inverse design approach searches for an aerofoil shape until the requirements for particular flow characteristic such as pressure distributions and skin friction are fulfilled (Della Vecchia *et al.* 2014).

The aerofoil shape can be represented by several available parametrisation techniques such as the widely used B-splines, Bezier, and PARSEC parametrisations (Della Vecchia *et al.* 2014; Derksen and Rogalsky 2010; Salunke *et al.* 2014). The shape parametrisations can affect the optimisation search and

should represent a wide range of aerofoil shapes (Derksen and Rogalsky 2010). In the PARSEC parametrisation, the aerofoil surface can be represented by two curves, one for the upper surface and the other for the lower surface. Each curve can be represent using parameters linked directly to the commonly-defined aerofoil section geometry such as the maximum thickness and its location, radius of the leading edge, thickness and direction angle of the trailing edge. These parameters should be selected carefully to achieve a reasonable aerofoil section, during the optimisation search, capable to be solved by the aerodynamic solver. The range of their values must be selected carefully in order to prevent unnecessary reflex in the upper and lower surfaces generating unreasonable aerofoil shape thus delaying the convergence of optimisation. A methodology for this parametrisation is presented by Sobieczky (1997). Another popular parametrisation is called Bezier curve techniques, representing the aerofoil surfaces by two curves, one for upper surface and the other for lower surface, or one for camber line and the other for thickness distribution. Bezier curve can be designed with using its controlled point which defining the curves shape (Derksen and Rogalsky 2010; Park *et al.* 2008; Salunke *et al.* 2014). Several approaches aiming to enhance the trailing and leading edge shapes representation were introduced using multi curve with number of variables. The number of these curves and their

point's coordinates can extremely affect the resolution and optimisation of time consumption (Della Vecchia *et al.* 2014; Salunke *et al.* 2014). Derksen and Rogalsky (2010) introduced a new aerofoil parametrisation (Bezier-PARSEC): the Bezier parametrisation which was used to represent the aerofoil edges, and the PARSEC approach to represent rest of the aerofoil surface. The aim was to enhance the matching of representing a wide number of existing aerofoils in addition to accelerate the speed converge of aerodynamic solver (Derksen and Rogalsky 2010). In this paper, the PARSEC parametrisation is chosen to represent the camber line of the aerofoil and the Bezier curve for the thickness distribution. This combination looks efficient as observed during the optimisation process and the generated aerofoils were reasonable.

AEROFOIL SHAPE OPTIMISATION TOOL

Numerous aerofoils of different thickness have been designed using a MATLAB tool, which has been coded as a part of this paper. This tool consists of 2 parts in addition to the aerodynamic solver (XFOIL), as shown in Fig. 2. The first part generates the aerofoil section geometry using a combination of PARSEC and Bezier-curve parameterisation developed in this paper, involving 9 variables shown in Fig. 3. The second part contains the optimisation code using the canonical genetic algorithm, while several optimisation algorithms can be used within the MATLAB environment.

AEROFOIL SHAPE PARAMETERISATION

A combination of PARSEC and Bezier-Curve has been used to represent the aerofoil surface. In this paper, the PARSEC parameterisation is used to represent the camber line of the aerofoil, while the Bezier-Curve is used to represent the thickness distribution. The reason of using this combination is to achieve reasonable aerofoil geometries during the optimisation process and to prevent unconvergence problem of the aerodynamic solver, thus improving the time consumption and program stability. Moreover, by Bezier-Curve, the thickness distribution can easily be constrained to achieve a positive distribution, in addition to achieving a specific maximum aerofoil thickness. As experience was obtained during this study, it has been found that this combination is efficient to search for the optimised setting because of its capability to define a set of proper design variables leading to a rapid convergence.

Thickness Distribution

Bezier-Curve parameterisation has been used to represent the thickness distribution of the section, and the curve can be represented by associated control points. The generated curve passes through the first and last control points, but does not need to pass through the other control points.

Assume a number of control points (n), with their coordinates $P(xc_i, b_i)$, where b_i will be denoted as Bezier parameters while xc_i are set as in Fig. 3a. The curve can be discretised into a number of segments; each segment length will be denoted as (t),

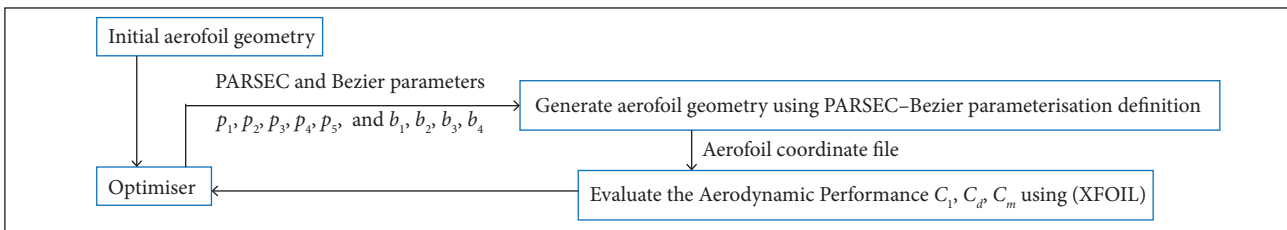


Figure 2. Aerofoil shape optimisation flow.

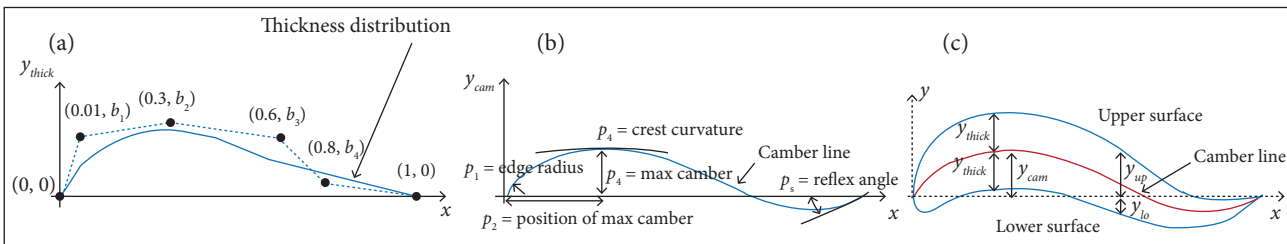


Figure 3. PARSEC-Bezier parameterisation definition. (a) Bezier curve for thickness distribution; (b) PARSEC parameterisation for camber line; (c) Aerofoil surface.

where $0 \leq t \leq 1$. The blending function of each segment can be evaluated by:

$$B_i^n = \frac{n!}{i!(n-i)!} (1-t)^{n-i} t^i \quad (1)$$

The coordinates of each segment of the curve () associated with the given control points are found by:

$$X_{thick}(t) = \sum_{i=1}^n x c_i B_i^n(t)$$

and

$$Y_{thick}(t) = \sum_{i=1}^n b_i B_i^n(t)$$

where: Y_{thick} represents the distribution of the half thickness of the aerofoil along the x -coordinate; X_{thick} represents the x -coordinate of the upper and the lower surface.

Camber Line

PARSEC parameterisation has been used to represent the camber line of the aerofoil. In this paper, only 1 curve of the PARSEC parametrisation is taken. This curve can be represented by associated geometry parameters of the camber line (p_1, p_2, p_3, p_4, p_5), as defined in Fig. 3b. According to the PARSEC methodology, the vertical coordinates of the curve at a given (x) coordinate location is given by:

$$Y_{cam}(x) = \sum_{i=1}^{n=5} a_{pa}^i \cdot x^{i-\frac{1}{2}} \quad (3)$$

The coefficients a_{pa} are calculated from the 5 parameters (p_1, p_2, \dots, p_5) of the aerofoil camber as follows:

$$b_{pa} = a_{pa} \times C_{pa} \quad (4)$$

where $b_{pa} \wedge C_{pa}$ are evaluated from the following matrices:

$$C_{pa} = \begin{pmatrix} 1 & 1 & 1 & 1 & 1 & 1 \\ p_2^{0.5} & p_2^{1.5} & p_2^{2.5} & p_2^{3.5} & p_2^{4.5} & p_2^{5.5} \\ 0.5 & 1.5 & 2.5 & 3.5 & 4.5 & 5.5 \\ 0.5p_2^{-0.5} & 1.5p_2^{0.5} & 2.5p_2^{1.5} & 3.5p_2^{2.5} & 4.5p_2^{3.5} & 5.5p_2^{4.5} \\ -0.25p_2^{-1.5} & \frac{3}{4}p_2^{-0.5} & \frac{15}{4}p_2^{0.5} & \frac{15}{4}p_2^{1.5} & \frac{63}{4}p_2^{2.5} & \frac{99}{4}p_2^{3.5} \\ 1 & 0 & 0 & 0 & 0 & 0 \end{pmatrix}, \quad (5)$$

$$b_{pa} = \begin{pmatrix} 0 \\ p_3 \\ \tan(p_3/2) \\ 0 \\ p_4 \\ \sqrt{2p_1} \end{pmatrix} \quad (5)$$

Then, the y -coordinates of the upper and lower surfaces can be calculated as shown in Fig. 3c by:

$$y_{up}(x) = Y_{cam}(x) + Y_{thick}(x) \quad (6)$$

$$y_{lo}(x) = Y_{cam}(x) - Y_{thick}(x) \quad (7)$$

Therefore, the aerofoil surface will be defined regarding the Bezier and PARSEC parameters, with 9 variables: .

The Aerodynamic Solver

XFOIL has been used as the aerodynamic solver of the optimisation tool. It is a 2-D aerodynamic solver widely used in the design and optimisation of aerofoils due to its ability to produce good and rapid solutions that can be obtained to match experimental data. It is a combination of inviscid-viscous flow analyses where some approximations are performed. The input parameters of this solver are the aerofoil coordinates and the flow conditions, such as the AoA and Reynolds number.

Problem Formulation

The primary target was to design a number of aerofoils, with low pitching moment, suitable for an aft-swept flying wing configuration, operating at low Reynolds number of about 0.5×10^6 . Three optimisation targets were set to achieve maximum aerodynamic performance characteristics. Each individual target is run separately to design several aerofoils of different thicknesses that meet the target criteria. The set targets are:

- To achieve maximum lift/drag ratio with no less than a pitching moment coefficient of -0.05 :

$$\text{maximize } (C_l/C_d)$$

$$\text{subject: } C_m > -0.05$$
- To achieve maximum lift/drag ratio with no less than a pitching moment coefficient of -0.02 :

$$\text{maximize } (C_l/C_d)$$

$$\text{subject: } C_m > -0.02$$

- To achieve maximise ($C_l^{1.5}/C_d$) ratio with no less than a pitching moment coefficient of -0.05 :

$$\text{maximize } (C_l^{1.5}/C_d)$$

$$\text{subject: } C_m > -0.05$$

The design variables of the optimisation problems are the PARSEC and Bezier parameters: $p_1, p_2, p_3, p_4, p_5, b_1, b_2, b_3, b_4$.

In each design target, the thickness of the optimal aerofoil is constrained during the optimisation to offer different aerofoils with different thicknesses. The constraining is done by controlling the upper and the lower bounds of the Bezier parameter values (b_1, b_2, b_3, b_4). The flow condition was set at an AoA of 6° and Reynolds number of 0.5×10^6 .

NEWLY DESIGNED AEROFOILS

Table 2 shows the aerodynamic performance of the newly designed aerofoils at the maximum lift/drag ratio in addition to the maximum and minimum lift coefficients and stall angles. Their names and numbers are temporarily used at this stage of study and they have no other meanings. The shapes and aerodynamic characteristics of some of the newly designed aerofoils are shown in Fig. 4 at Reynolds number of 5×10^5 .

According to the set of results obtained so far, as tabulated in Table 2 and Fig. 4, the overall observations of the optimised aerofoils can be summarised as follows:

- The lift/drag ratios are higher than corresponding existing aerofoils presented in Table 1, and this is expected because the pitching moment of the new aerofoils is higher than of those in Table 1.
- Increasing the maximum thickness of the aerofoil leads to a decrease in the maximum lift/drag ratio.
- For thicker aerofoils such as ZMR-16, ZMR-18, and ZMR-19, the lift/drag ratio per AoA slopes sharply drops after the maximum value.
- The variation of the pitching moment with the AoA is not smooth in some of the optimised aerofoils, but this could be suspicious because the pitching moment of XFOIL results could be inaccurate. Other aerodynamic solver or experimental study will be needed to verify this behaviour.
- The stall angles are not close to the angles in which the maximum lift/drag ratio is achieved.
- Reducing the pitching moments result in reduction of the maximum lift/drag ratio and increased drag (see ZMR-26 and ZMR-27 in Table 2).

It is worth mentioning that the maximum C_l is not employed in the optimisation target and the focus was at an AoA of 6° for maximum lift/drag ratio away from the stall angle. Therefore, most of the newly designed aerofoils would have stalled at about 8° from the angle corresponding to the

Table 2. Aerodynamic performance of the new aerofoils at $Re = 0.5 \times 10^6$, obtained by XFOIL.

| Aerofoil name | At max C_l/C_d | | | | | C_{lmax} | C_{lmin} | Stall angle | Thickness t/c [%] |
|---|------------------|-------|---------|---------|------------------|------------|------------|-------------|---------------------|
| | C_l/C_d | C_l | C_d | C_m | At AoA \approx | | | | |
| max C_l/C_d $C_m > -0.05$ | | | | | | | | | |
| ZMR-9 | 117.9 | 1.081 | 0.0091 | -0.0497 | 6 | 1.34 | -0.37 | 15 | 9.9 |
| ZMR-12 | 115.4 | 0.980 | 0.0085 | -0.0497 | 6 | 1.25 | -0.418 | 14 | 12.71 |
| ZMR-13 | 109.4 | 0.96 | 0.0087 | -0.0482 | 6 | 1.24 | -0.52 | 15 | 14.44 |
| ZMR-14 | 111.1 | 1.051 | 0.0094 | -0.0493 | 6 | 1.3 | -0.31 | 15 | 16.6 |
| ZMR-15 | 95.04 | 0.99 | 0.0104 | -0.0445 | 6 | 1.202 | -0.41 | 18 | 20.91 |
| max $C_l^{1.5}/C_d$ $C_m > -0.05$ | | | | | | | | | |
| ZMR-20 | 120.8 | 1.135 | 0.0094 | -0.0496 | 6 | 1.448 | -0.293 | 17 | 9.11 |
| ZMR-17 | 117.6 | 1.191 | 0.0101 | -0.049 | 7 | 1.446 | -0.48 | 15 | 12.57 |
| ZMR-19 | 114.7 | 1.056 | 0.0092 | -0.0498 | 6 | 1.388 | -0.34 | 16 | 15.02 |
| ZMR-18 | 114 | 1.149 | 0.0093 | -0.049 | 7 | 1.435 | -0.49 | 16 | 15.83 |
| ZMR-16 | 95.51 | 1.017 | 0.0106 | -0.0443 | 6 | 1.296 | -0.388 | 17 | 20.68 |
| max C_l/C_d $C_m > -0.02$ | | | | | | | | | |
| ZMR-26 | 93.91 | 1.268 | 0.0139 | -0.0181 | 7 | 1.495 | -1 | 15 | 14.91 |
| ZMR-27 | 80.52 | 1.234 | 0.01532 | 0.0341 | 10 | 1.46 | -1.152 | 14 | 15.57 |

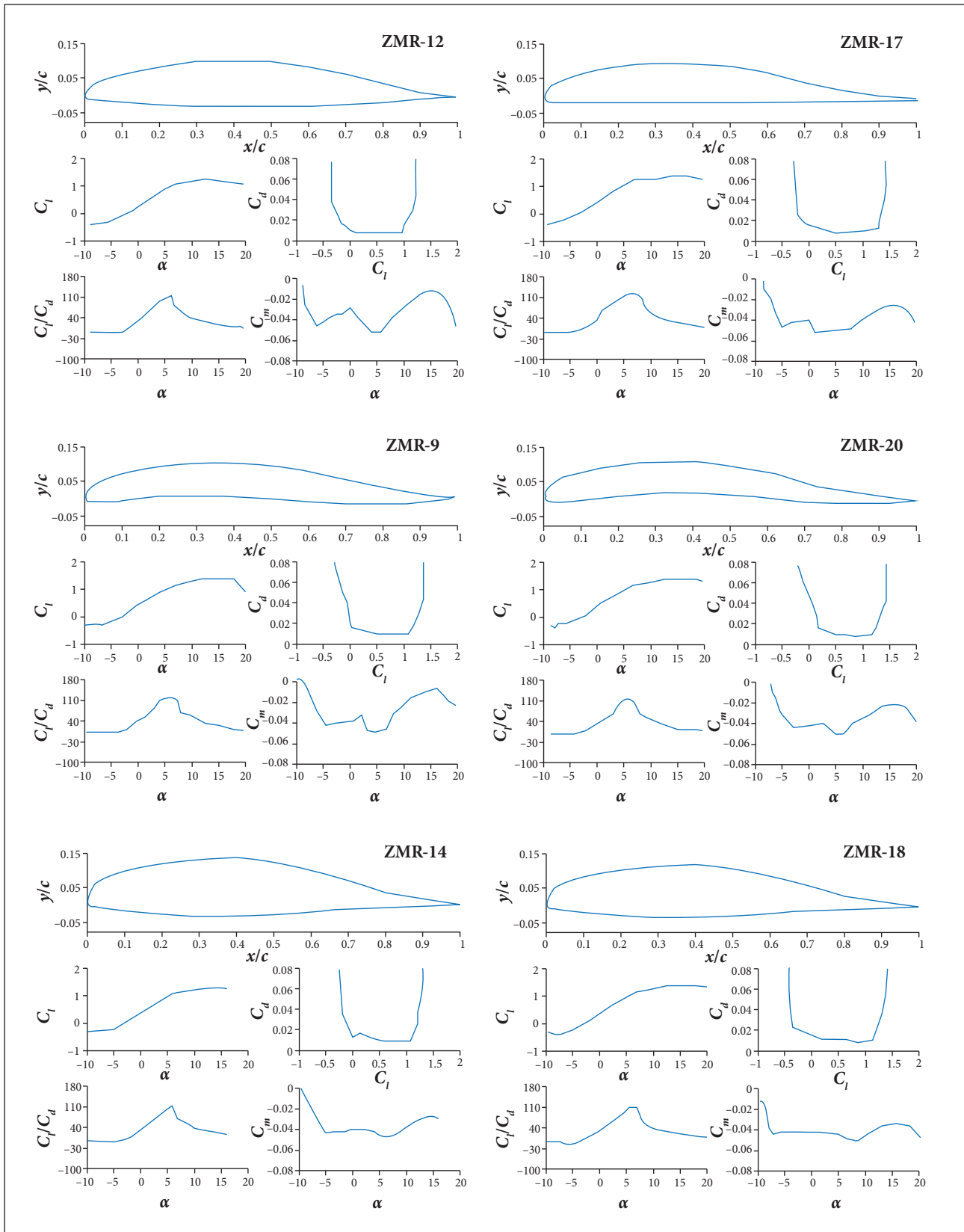


Figure 4. Aerodynamic performance of the newly designed aerofoils at $Re = 0.5 \times 10^6$.

maximum lift/drag ratio. ZMR-26 and ZMR-19 are the most interesting aerofoils for the authors as they will be candidate for an aft-swept aircraft due to their moderate thicknesses and the high maximum lift/drag ratios. They will be validated by a high order analysis solver in the next section.

COMPUTER FLUID DYNAMICS MODEL

High-order Computer Fluid Dynamics (CFD) analysis has been conducted to validate some of the newly designed aerofoils using FLUENT ANSYS. Aerofoils ZMR-19 and ZMR-26 are selected to this study due to their moderate thickness intended to be adopted for a high altitude aft-swept flying wing configuration in future work. A C-type mesh is adopted with a proper mesh density to ensure that Y^+ of the first row of cells adjacent to the aerofoil surface is less than one. Figure 5 shows the schematic of a partial domain of ZMR-19. The boundary conditions are the upper and the lower flow domain boundary as a function of the velocity-inlet boundary whilst the downstream is considered as a pressure-outlet boundary. In addition, the aerofoil surface is considered as a wall. The SST $k-\omega$ (4eq) model, which can predict laminar-to-turbulent transition, is used due to its accuracy for a wide class of flows (Ansys® 2013). The

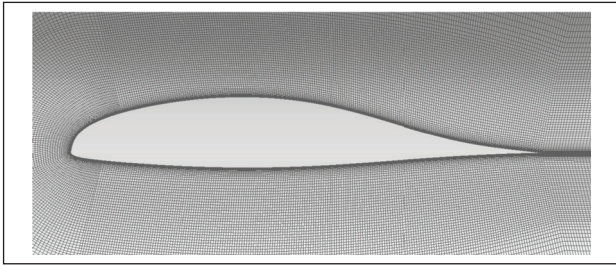


Figure 5. Schematics of the partial domain of ZMR-19.

calculations are carried out at chord-base Reynold number of 0.5×10^6 .

RESULTS AND DISCUSSION

High-order analyses have been conducted to validate the aerodynamic performance of ZMR-19 and ZMR-26 aerofoils. The XFOIL predictions show that lift, drag, and pitching moment coefficients are in good agreement with FLUENT at low AoAs as shown in Figs. 6 and 7. However, at higher AoAs near the stall region, XFOIL predictions have not shown the same behaviour, especially the pitching moment coefficient.

Figures 8 and 9 show laminar separations (LS) of the ZMR-19 which occur at the upper and lower surfaces of the aerofoil at $AoA = 0^\circ$. At an AoA equal to 6° , where the maximum lift/drag ratio is achieved, the LS of the lower surface has disappeared, while the separation bubble at the upper surface has slightly migrated forwards. Since the magnitudes of the velocity vectors within the bubble are small, the scales of the vectors shown in the figures were set to 4.

The flow around the ZMR-26 aerofoil also shows similar behaviour as seen in the lower surface at $AoA = 0^\circ$ (Fig. 10). On the other hand, in Fig. 11, at an AoA of 6° , the LS has vanished, and the flow remains attached all the way to the trailing edge. Nevertheless, the LS was also observed in existing aerofoils such as the LA2573A section, which is used in the NASA prototypes Helios and Pathfinder. The velocity contour and vector for the flow around the LA2573A section are shown in Figs. 12 and 13. Figure 12 illustrates the LS at the lower surface, which occurs at $AoA = 0^\circ$. At 10° , where the maximum lift/drag ratio is achieved, the LS on the upper surface becomes noticeable as shown in Fig. 13.

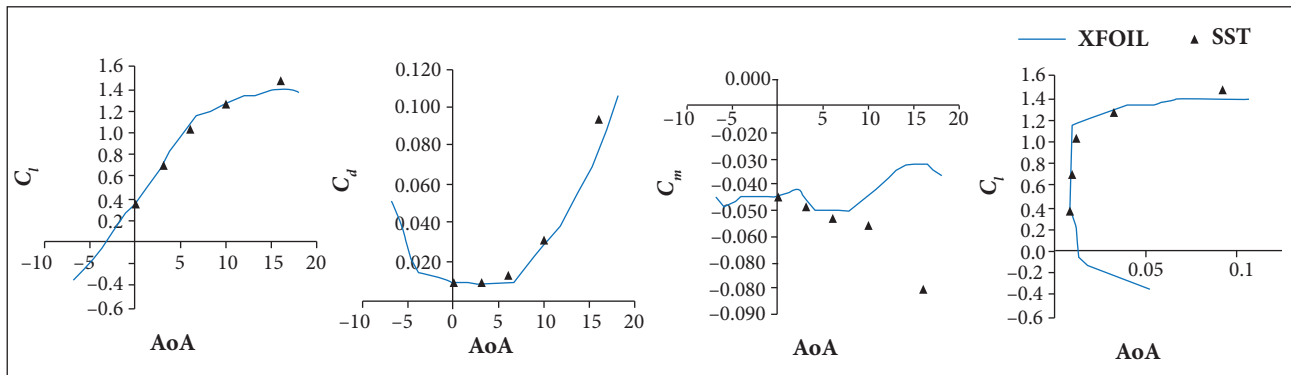


Figure 6. Aerodynamic performance of ZMR-19 aerofoil using SST $k-\omega$ (4eq) model and XFOIL at $Re = 0.5 \times 10^6$.

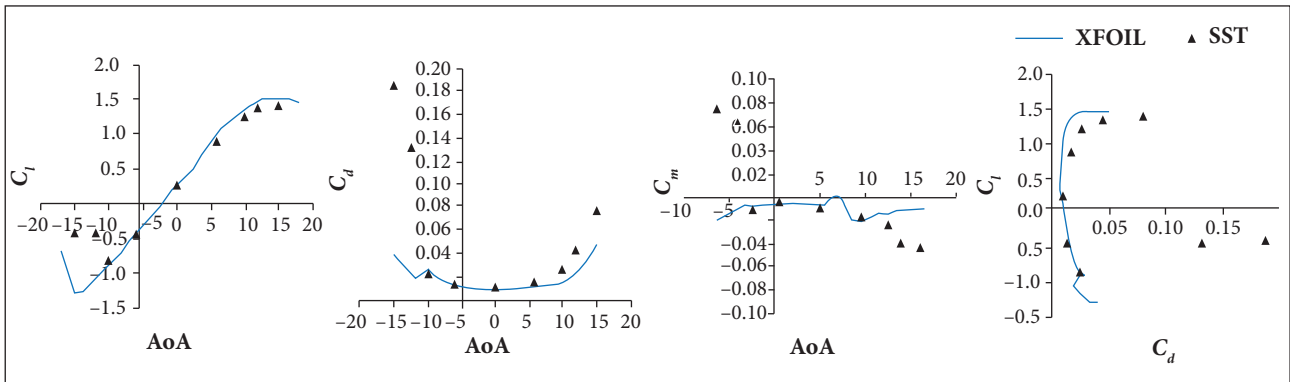


Figure 7. Aerodynamic performance of ZMR-26 aerofoil using SST $k-\omega$ (4eq) model and XFOIL at $Re = 0.5 \times 10^6$.

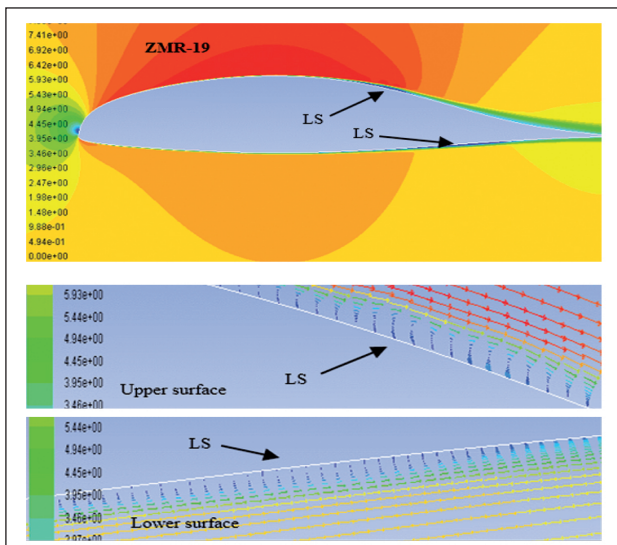


Figure 8. Velocity contour and vector at $AoA = 0^\circ$ of ZMR-19 aerofoil.

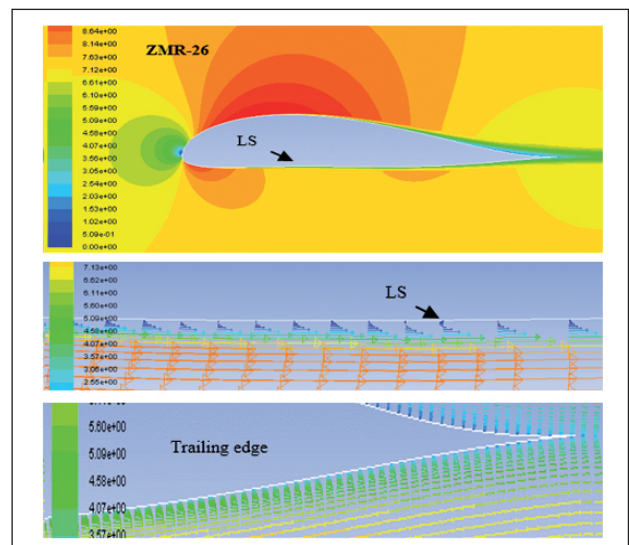


Figure 10. Velocity contour and vector at $AoA = 0^\circ$ of ZMR-26 aerofoil.

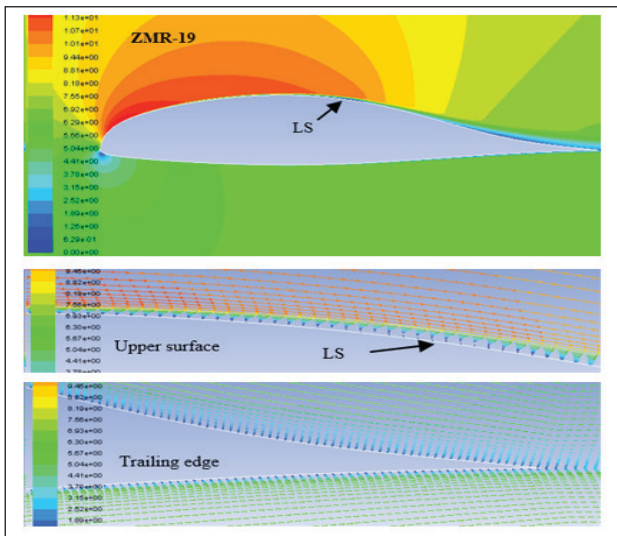


Figure 9. Velocity contour and vector at $AoA = 6^\circ$ of ZMR-19 aerofoil.

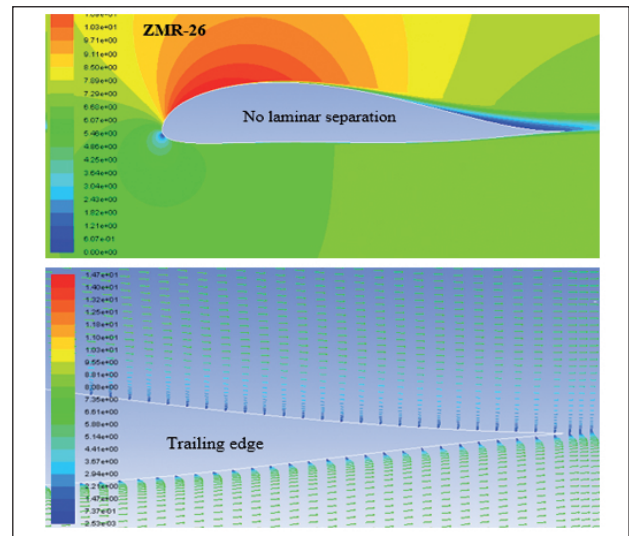


Figure 11. Velocity contour and vector at $AoA = 6^\circ$ of ZMR-26 aerofoil.

It is concluded that, at low Reynolds number, the LS could occur on both surfaces at small AoAs. As the AoA increases, LS bubbles either begin to disappear or move forward. The intensity of the predicted bubbles was small

and hence they are not expected to have pronounced effects on performance.

CONCLUSION

A number of new aerofoils with varying thicknesses for an aft-swept flying wing UAV, operating at low Reynolds number of about , have been designed using a developed aerofoil parametrisation employed in the optimisation tool. The aerodynamic performance of the newly designed aerofoil shows that the maximum lift/drag ratio is affected by the thickness-to-chord ratio. Increasing the maximum thickness of the aerofoil leads to a decrease in the maximum lift/drag ratio. In addition, as expected, this ratio sharply drops in value after the maximum is reached. The stall angles of these aerofoils are not close to the corresponding angle of the maximum lift/drag ratio. LS, especially at small AoAs, was observed in the ZMR-19 and ZMR-26 aerofoils. However, this was also observed in existing aerofoils such as the LA2573A. Further optimisation processes and validation by experimental tests will be carried out within the discussed range of Reynolds numbers to instil confidence.

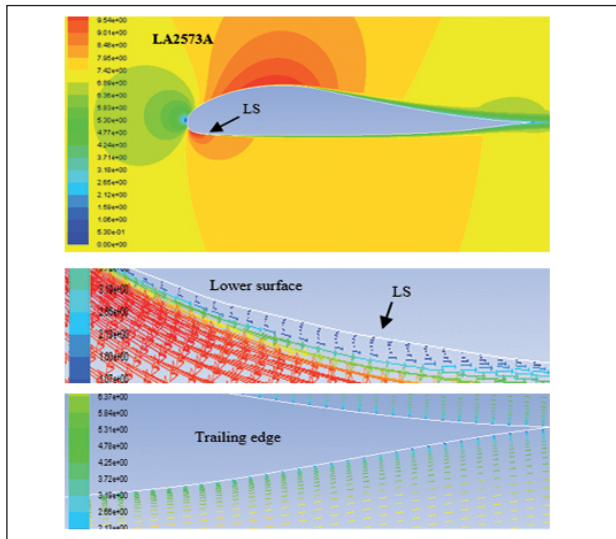


Figure 12. Velocity contour and vector at AoA = 0° of LA2573A aerofoil.

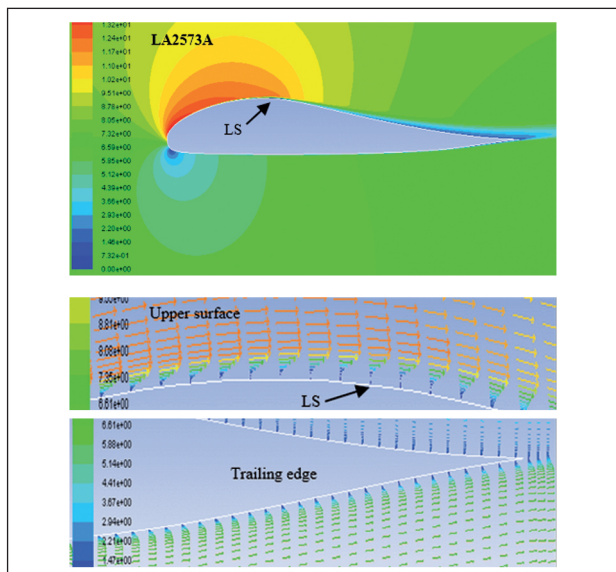


Figure 13. Velocity contour and vector at AoA = 10° of LA2573A aerofoil.

ACKNOWLEDGMENTS

The authors appreciate the Higher Committee of Education of Iraq (HCED-IRAQ) for supporting this study at the University of Salford.

AUTHOR'S CONTRIBUTION

Alsahlan AA conducted the study under the supervision of Rahulan T; both authors discussed the results and commented on the manuscript.

REFERENCES

Alsahlani A, Johnston LJ, Atcliffe PA (2015) Design of a high altitude long endurance flying-wing solar-powered unmanned air vehicle.

Proceedings of the 6th European Conference for Aeronautics and Space Sciences; Krakow, Poland.

- ANSYS® (2013) ANSYS FLUENT theory guide; [accessed 2017 Apr. 25]. <http://www.ansys.com>
- Buckstrom A (1979) The elements of tailless airplane design. *Sport Aviation* 5:39-44.
- Cerra DF, Katz J (2008) Design of a high-lift, thick airfoil for unmanned aerial vehicle applications. *J Aircraft* 45(5):1789-1793. doi: 10.2514/1.36924
- Della Vecchia P, Daniele E, D'Amato E (2014) An airfoil shape optimization technique coupling PARSEC parameterisation and evolutionary algorithm. *Aero Sci Tech* 32(1):103-110. doi: 10.1016/j.ast.2013.11.006
- Derksen R, Rogalsky T (2010) Bezier-PARSEC: An optimized aerofoil parameterisation for design. *Adv Eng Software* 41(7-8):923-930. doi: 10.1016/j.advengsoft.2010.05.002
- Greer D, Hamory P, Edwards C, Krake K, Drela M (2000) Design and predictions for high-altitude (low Reynolds number) aerodynamic flight experiment. *J Aircraft* 37(4):684-689. doi: 10.2514/2.2652
- Hazra SB, Jameson A (2007) Aerodynamic shape optimization of airfoils in ultra-low Reynolds number flow using simultaneous pseudo-time stepping. Aerospace Computing Lab (ACL) Report, 2007-4; [accessed 2017 Apr. 25]. http://aero-comlab.stanford.edu/Papers/lowren_paper.pdf
- Kroo I (1993) Tailless aircraft design — recent experiences. *Proceedings of the Symposium on Aerodynamics and Acoustics*; New Jersey, USA.
- Lei J, Guo F, Huang C (2013) Numerical study of separation on the trailing edge of a symmetrical airfoil at a low Reynolds number. *Chin J Aeronaut* 26(4):918-925. doi: 10.1016/j.cja.2013.06.005
- Li P, Zhang B, Chen Y, Yuan C, Lin Y (2012) Aerodynamic design methodology for blended wing body transport. *Chin J Aeronaut* 25(4):508-516. doi: 10.1016/s1000-9361(11)60414-7
- Lissaman P (1983) Low-Reynolds-number airfoils. *Annual Review of Fluid Mechanics* 15(1):223-239. doi: 10.1146/annurev.fl.15.010183.001255
- Ma R, Liu P (2009) Numerical simulation of low-Reynolds-number and high-lift airfoil S1223. *Proceedings of the World Congress on Engineering*; London, UK.
- Mader C, Martins J (2012) Optimal flying wings: a numerical optimization study. *Proceedings of the 53rd AIAA/ASME/ASCE/AHS/ASC Structures, Structural Dynamics, and Materials Conference*; Honolulu, USA.
- McArthur J (2007) Aerodynamics of wings at low Reynolds numbers (PhD thesis). Los Angeles: University of Southern California.
- Nickel K, Wohlfahrt M (1994) *Tailless aircraft in theory and practice*. Washington: American Institute of Aeronautics and Astronautics.
- Park K, Han JW, Lim HJ, Kim BS, Lee J (2008) Optimal design of airfoil with high aspect ratio in Unmanned Aerial Vehicles. *Proceedings of the World Academy of Science: Engineering and Technology* 42:182.
- Qin N, Vavalle A, Le Moigne A, Laban M, Hackett K, Weinerfelt P (2004) Aerodynamic considerations of blended wing body aircraft. *Progr Aero Sci* 40(6):321-343. doi: 10.1016/j.paerosci.2004.08.001
- Rapinett A (2009) *Zephyr: a high altitude long endurance Unmanned Air Vehicle* (Master's thesis). Surrey: University of Surrey.
- Salunke NP, Juned Ahamad RA, Channiwala SA (2014) Airfoil parameterization techniques: a review. *Am J Mech Eng* 2(4):99-102. doi: 10.12691/ajme-2-4-1
- Sobieczky H (1997) *Geometry generator for CFD and applied aerodynamics. Courses and Lectures - International Centre for Mechanical Sciences* 366:137-158.
- The Guardian (2015) Facebook launches Aquila solar-powered drone for internet access; [accessed 2016 May 3]. <https://www.theguardian.com/technology/2015/jul/31/facebook-finishes-aquila-solar-powered-internet-drone-with-span-of-a-boeing-737>